Paper AAS 04-157

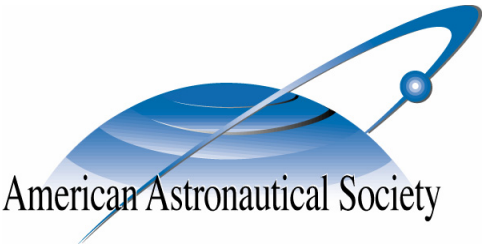

ASPHERICAL FORMATIONS NEAR THE LIBRATION POINTS IN THE SUN-EARTH/MOON EPHEMERIS SYSTEM

B. G. Marchand and K. C. Howell
School of Aeronautics and Astronautics, Purdue University
West Lafayette, Indiana 47907-1282

14th AAS/AIAA Space Flight Mechanics Conference

Maui, Hawaii **February 8-12, 2004**

AAS Publications Office, P.O. Box 28130, San Diego, CA 92198

AAS 04-157

ASPHERICAL FORMATIONS NEAR THE LIBRATION POINTS IN THE SUN-EARTH/MOON EPHEMERIS SYSTEM

B.G. Marchand [*] and K.C. Howell [†]

Multi-spacecraft formations, evolving near the vicinity of the libration points of the Sun-Earth/Moon system, have drawn increased interest for a variety of applications. This is particularly true for space based interferometry missions such as TPF and MAXIM. The present study considers both continuous and discrete control methods as applied to non-natural formation configurations. Continuous output feedback linearization methods are employed to enforce non-natural configurations. The general focus is around multi-spacecraft formations that are constrained to evolve along an aspherical surface, such as a paraboloid, such that the orientation of the formation is fixed in inertial space. Also, a discrete Floquet controller, previously developed for the determination of natural formations, is further investigated. Its application to inertially fixed formations is of particular interest. The general development is presented in the Sun-Earth/Moon ephemeris model.

INTRODUCTION

The dynamical sensitivity that is characteristic of the region near the libration points, combined with the path constraints usually imposed on the envisioned nominal formation configurations, makes formation keeping and deployment an interesting and challenging problem. Although some preliminary analyses have already been completed [1-15], a better understanding of natural and controlled formations in this region of space is still necessary. In previous work, Howell and Marchand [13-14] consider both continuous and impulsive control to enforce a variety of non-natural formations. Among these, inertially fixed configurations are of particular interest for space based interferometry.

[*] Graduate Student, School of Aeronautics and Astronautics, Purdue University, West Lafayette, IN 47906
[†] Professor, School of Aeronautics and Astronautics, Purdue University, West Lafayette, IN 47906

Continuous control techniques, such as Linear Quadratic Regulator (LQR), nonlinear optimal control, and feedback linearization methods, are successfully applied to this type of formation [13-14]. Although the mathematical implementation of these control laws is effective, the resulting control accelerations can be prohibitively small, depending on the desired configuration. For instance, near the libration points, formations that require the deputy vehicle to remain at a constant distance and orientation, relative to the chief spacecraft, are associated with thrust levels on the order of 0.81-3.21 nN, for a 10 meter separation and a 700 kg vehicle. Increasing the nominal separation by one order of magnitude also increases the cost by one order of magnitude. This indicates that a 10,000 km separation is required, for this type of formation, in order for the thrust level to exceed 1 μN of nominal thrust. The present state of propulsion technology allows for operational thrust levels on the order of 90-1000 μN via pulsed plasma thrusters, such as those available for attitude control onboard EO-1 [16]. Increased interest in micro- and nano-satellites continues to motivate theoretical and experimental studies to further lower these thrust levels, as discussed by Mueller [17], Gonzalez [18] and Phipps [19]. Gonzalez [18] estimates that a lower bound of 0.3 nN is possible via laser induced ablation of aluminum. Aside from their immediate application to micro- and nano-satellite missions, these concepts are also potentially promising for formation flight near the libration points. However, the presently available technology may be sufficient to pursue other types of formation flight configurations, such as those presented here and in previously considered sample formations [14]. In particular, configurations that require the deputy vehicle to spin, relative to the chief, at some fixed rate, such as those presently and previously considered by Marchand and Howell [14], can quickly drive the thrust levels into the mN range.

Of course, continuous thruster operation may not always represent a feasible option. In such a case, the formation keeping task must rely on a discretized approach. Mathematically, a standard targeter approach [14] can accomplish the goal to within a reasonable degree of accuracy, provided the nominal vehicle separations are on the order of meters. However, because these configurations are not consistent with the natural dynamics near the libration points, the error incurred between maneuvers grows rapidly as this nominal separation increases. Furthermore, the size of the maneuvers can still be prohibitively small.

The continuous control laws previously presented [13-14] and the discrete targeter approach [14] have something in common. Both of these methods try to force configurations that are not consistent with the natural dynamics and they can both require unreasonably small thrust levels, depending on the constraints on the configuration. This is not surprising given the highly sensitive nature of the dynamics. To circumvent this difficulty, it is advantageous to develop a better understanding of the natural formation

dynamics near the libration points and incorporate such knowledge in the design of both the nominal configurations and the associated control laws. In one such example, Howell and Marchand [14] successfully identify a series of naturally existing formations, as well as deployment into these configurations, through the use of a modified Floquet controller. These naturally existing formations evolve in the vicinity of a reference "halo" orbit near the L_1 and L_2 libration points of the Sun-Earth/Moon system. The resulting control law is based on knowledge of the linear stability of the reference orbit. In particular, the controller is designed to remove the unstable mode as well as two of the four center modes associated with the "halo" orbit.

In the present effort, the natural formations previously identified in the CR3BP [14], via the Floquet approach, are transitioned into the more complete ephemeris model. A constrained two-level differential corrector is then applied to these solutions to enforce periodicity in the ephemeris model via small impulsive maneuvers applied once a year. Further application of this methodology as a design tool to identify inertially fixed formations is of particular interest. Also, continuous output feedback linearization methods, previously considered in [14], are similarly employed. The focus is multi-spacecraft formations that are constrained to evolve along an aspherical surface, such as a paraboloid, fixed in inertial space. The development is presented in the Sun-Earth/Moon ephemeris model. Potentially, these two approaches can be combined into one formation keeping strategy, particularly for formations that do not require the nominal configuration to be enforced at all times. For instance, the Floquet controller can be used to drive the vehicles onto a naturally existing formation via a single impulsive maneuver until a reconfiguration, that requires continuous control, is necessary.

DYNAMICAL MODEL

Background

In this investigation, the standard form of the relative equations of motion for the *n*-body problem, as formulated in the inertial frame (I), is employed. The effects of solar radiation pressure (SRP) are also incorporated. Hence, the dynamical evolution of each vehicle in the formation is governed by

$$ {}^{I}\ddot{\bar{r}}^{P_2P_s} = \bar{f}_{grav}^{(P_s)} + \bar{f}_{srp}^{(P_s)} + \bar{u}(t). \tag{1.1} $$

For notational purposes, let P_2 denote the central body of integration, in this case the Earth. Then, P_s identifies the spacecraft, $\bar{f}_{grav}^{(P_s)}$ represents the sum of all gravitational forces acting on P_s, $\bar{f}_{srp}^{(P_s)}$ is the force exerted on the vehicle due to solar radiation pressure, and $\bar{u}(t)$ is the control input vector.

From this general expression, the equations of motion for both the chief and deputy spacecraft may be expressed in the following form,

$$ {}^{I}\ddot{\bar{r}}_I^{P_2C} = \bar{f}_{grav}^{(C)} + \bar{f}_{srp}^{(C)} + \bar{u}_C(t) = \bar{f}^{(C)} + \bar{u}_C(t), \tag{1.2} $$

$$ {}^{I}\ddot{\bar{r}}_I^{P_2D_i} = \bar{f}_{grav}^{(D_i)} + \bar{f}_{srp}^{(D_i)} + \bar{u}_{D_i}(t) = \bar{f}^{(D_i)} + \bar{u}_{D_i}(t), \tag{1.3} $$

where $\bar{u}_C(t)$ and $\bar{u}_{D_i}(t)$ denote the control accelerations required to maintain the desired nominal configuration, and $\bar{f}^{(C)}$ and $\bar{f}^{(D_i)}$ represent the net force acting on the chief spacecraft and the i^{th} deputy vehicle, respectively. The numerical integration for all vehicles in the formation is performed in terms of inertial coordinates. Define the measure numbers of a position vector such that $\bar{r}^{P_2D_i} = x_i\hat{X} + y_i\hat{Y} + z_i\hat{Z}$. Hence, the vehicle velocities and accelerations are associated with the inertial frame (*I*) defined in terms of the unit vectors $\hat{X}$, $\hat{Y}$, and $\hat{Z}$.

The chief spacecraft is assumed to evolve along a quasi-periodic Lissajous trajectory. Since this is a naturally existing solution in this regime, the baseline control acceleration $\bar{u}_C(t)$ is zero. The relative equations of motion for the i^{th} deputy, then, are easily determined by subtracting Equation (1.2) from (1.3),

$$ {}^{I}\ddot{\bar{r}}_I^{CD_i} = \left(\bar{f}_{grav}^{(D_i)} - \bar{f}_{grav}^{(C)}\right) + \left(\bar{f}_{srp}^{(D_i)} - \bar{f}_{srp}^{(C)}\right) + \bar{u}_{D_i}(t) = \Delta\bar{f}^{(D_i)} + \bar{u}_{D_i}(t). \tag{1.4} $$

The vector $\bar{r}^{CD_i}$ denotes the position of the i^{th} deputy relative to the chief spacecraft while $\Delta\bar{f}^{(D_i)}$ represents the relative net force vector.

Let $\bar{\rho}_I$ represent the desired nominal path of the deputy spacecraft, then, ${}^I\dot{\bar{\rho}}_I$ designates the nominal velocity vector, and $\bar{u}_{D_i}{}^{\circ}(t)$ denotes the associated nominal control effort such that,

$$ {}^I\ddot{\bar{\rho}}_I = \Delta\bar{f}^{D_i^{\circ}} + \bar{u}_{D_i}{}^{\circ}(t) . \tag{1.5} $$

In this expression, the superscript $(\circ)$ implies evaluation on the nominal path defined by $\bar{\rho}_I$ and ${}^I\dot{\bar{\rho}}_I$.

SPHERICAL FORMATIONS – FIXED RADIAL DISTANCE AND ROTATION RATE

In previous studies [14-15] the application of output feedback linearization techniques to spherical formation configurations is considered. In the earlier formulation, only the radial distance between the chief and deputy vehicles is enforced while the orientation is left unconstrained. Hence, as long as the deputy spacecraft evolves along the surface of a sphere, whose radius is equal to the desired nominal separation, the goal for the controller is satisfied. Since only one variable is tracked, and there are three control inputs, an infinite number of solutions are available. Subsequently, the formation keeping costs can vary dramatically depending on the particular solution that is selected. The difference between each solution is reflected in the rotation rate and the orbital plane corresponding to the converged solution. For instance, the second column of Table 1 summarizes the controller formulations from the earlier analysis.

All four controllers in Table 1 accomplish the goal in terms of formation keeping, but the dynamical responses and the associated costs are significantly different. To better understand these differences, as identified by Howell and Marchand [14-15], consider, briefly, the instantaneous rotating frame defined by the radial vector from the chief spacecraft to the deputy ($\hat{r} = \bar{r}^{CD_i} \Big/ \left|\bar{r}^{CD_i}\right|$), the angular momentum direction ($\hat{h} = \left(\bar{r}^{CD_i} \times {}^I\dot{\bar{r}}^{CD_i}\right) \Big/ \left|\bar{r}^{CD_i} \times {}^I\dot{\bar{r}}^{CD_i}\right|$), and the corresponding tangential unit vector ($\hat{\theta} = \hat{h} \times \hat{r}$).

Table 1- OFL Control of Spherical Formations

Formulation	Control Law	Control Law in Terms Of Rotating Coordinates
1	$\bar{u}(t) = \dfrac{H(\bar{r},\dot{\bar{r}})}{r}\hat{r}$ Geometric Approach: Radial inputs only	$\bar{u}(t) = \dfrac{H(\bar{r},\dot{\bar{r}})}{r}\hat{r}$
2	$\bar{u}(t) = \left\{\dfrac{g(\bar{r},\dot{\bar{r}})}{r} - \dfrac{\dot{\bar{r}}^T\dot{\bar{r}}}{r^2}\right\}\bar{r} + \left(\dfrac{\dot{r}}{r}\right)\dot{\bar{r}} - \Delta\bar{f}(\bar{r})$	$\bar{u}(t) = (\cdots)\hat{r} + \left(\dot{r}\dot{\theta} - f_\theta\right)\hat{\theta} - f_h\hat{h}$
3	$\bar{u}(t) = \left\{\dfrac{1}{2}\dfrac{g(\bar{r},\dot{\bar{r}})}{r^2} - \dfrac{\dot{\bar{r}}^T\dot{\bar{r}}}{r^2}\right\}\bar{r} - \Delta\bar{f}(\bar{r})$	$\bar{u}(t) = (\cdots)\hat{r} - f_\theta\hat{\theta} - f_h\hat{h}$
4	$\bar{u}(t) = \left\{-rg(\bar{r},\dot{\bar{r}}) - \dfrac{\dot{\bar{r}}^T\dot{\bar{r}}}{r^2}\right\}\bar{r} + 3\left(\dfrac{\dot{r}}{r}\right)\dot{\bar{r}} - \Delta\bar{f}(\bar{r})$	$\bar{u}(t) = (\cdots)\hat{r} + \left(3\dot{r}\dot{\theta} - f_\theta\right)\hat{\theta} - f_h\hat{h}$

At any given time, the angular momentum vector provides information about the instantaneous relative orbital plane of the deputy vehicle ($\hat{h}$) as well as its rotation rate ($\dot{\theta}$) about $\hat{h}$. The rate of change of the relative angular momentum vector can be expressed in terms of this rotating coordinate system as

$$ {}^{I}\dot{\bar{h}} = \bar{r}^{CD_i} \times {}^{I}\ddot{\bar{r}}^{CD_i} = r\left(f_\theta + u_\theta\right)\hat{h} - r\left(f_h + u_h\right)\hat{\theta}\,, \tag{1.6} $$

where f_θ, f_h, u_θ, and u_h denote the components of $\Delta\bar{f}^{(D_i)}$ and $\bar{u}_{D_i}$ along the $\hat{\theta}$ and $\hat{h}$ directions, respectively. The associated unit normal vector, $\hat{h} = \bar{h}\left(\bar{h}^T\bar{h}\right)^{-1/2}$, varies with time as follows,

$$ {}^{I}\frac{d\hat{h}}{dt} = -\frac{r\left(f_h + u_h\right)}{h}\hat{\theta}\,. \tag{1.7} $$

Thus, the plane of motion is preserved, and completely determined by the relative initial state, if $u_h = -f_h$. The last column in Table 1 summarizes the $\hat{\theta}$ and $\hat{h}$ components of the control inputs listed in the second column. It is simple to show that, for the last three entries in Table 1, the plane of motion is preserved. Also, since $h = \left|\bar{h}\right| = r^2\dot{\theta}$, the rotation rate $\dot{\theta}$ is further determined by u_h . For instance, for the second case listed in Table 1, $u_\theta + f_\theta = \dot{r}\dot{\theta}$. While the radial distance converges to its final value, as commanded by the controller, the quantity $u_\theta + f_\theta \to 0$. Hence, $h \to h\left(t_f\right) = r_f\dot{\theta}_f$ and, thus, the rotation rate will converge on some limiting value. A similar statement can be made about the fourth entry in Table 1. Since the rotation rate is inversely proportional to the square of the radial distance, the formation keeping cost increases significantly for formations that seek to achieve nominal separations on the order of meters. The third entry in Table 1, however, is slightly different. In this case, it is determined that $u_\theta + f_\theta = 0$. This leads to $h(t) = r^2(t)\dot{\theta}(t) = h(0)$ and, consequently, the rotation rate along the surface of the sphere is <u>completely</u> determined by the initial relative state of the deputy at the time the controller is activated. For the case that employs radial axis inputs, that is, the first entry in Table 1, the $\hat{\theta}$ and $\hat{h}$ components of $\bar{u}_{D_i}$ are zero which leads to ${}^{I}\dot{\bar{h}} = rf_\theta\hat{h} - rf_h\hat{\theta}$. This indicates that, in general, and for an arbitrary set of initial conditions, neither the rotation rate nor the relative orbit normal are preserved with this type of control approach. However, if the nominal relative separation is small, it may <u>appear</u> that the solution converges onto a plane, though small deviations are present. These deviations are most visible at larger separations, on the order of hundreds or thousands of kilometers. These deviations are better visualized from the sample cases in Figure 1.

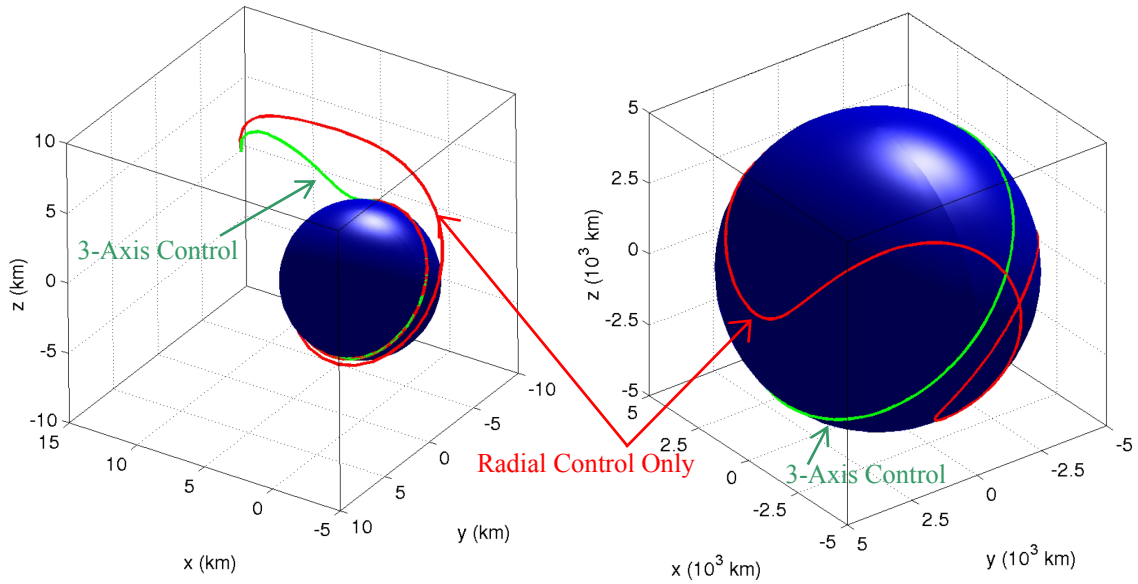

Figure 1 - Impact of Relative Orbit Size on Controlled Path of Deputy S/C
Radial Control Only/Free Orientation

The blue sphere in each subfigure represents the nominal surface. In Figure 1(a), the nominal distance is 5 km (the radius of the nominal sphere) as compared to 5000 km for the illustration in Figure 1(b). Each trajectory in Figure 1(a) is associated with an initial state characterized by $\bar{r}^{CD_i}(0) = [12 \quad -5 \quad 3]$ km and ${}^{I}\dot{\bar{r}}^{CD_i}(0) = [1 \quad -1 \quad 1]$ m/sec. The trajectories in Figure 1(b), are associated with the initial state $\bar{r}^{CD_i}(0) = [5007 \quad -5 \quad 3]$ km and ${}^{I}\dot{\bar{r}}^{CD_i}(0) = [1 \quad -1 \quad 1]$ m/sec. Both figures depict two separate paths evolving onto the nominal sphere. The green path is associated with the controller in the fourth entry of Table 1, while the red path is associated with the controller defined by radial axis inputs only, that is, the first entry in Table 1. Though numerical evidence may at times appear to suggest that each controller is converging onto the same orbital plane, as is apparent from Figure 1(a), the theoretical proof illustrates that radial axis inputs alone do not allow for this type of solution. This is evident from Figure 1(b).

Although preservation of the orbiting plane may be a desirable feature, the numerical and theoretical evidence clearly indicates the need to force the controller to track a particular rotation rate. Forcing a predetermined rotation rate prevents the dynamics from inducing a spin rate that may lead to prohibitively high formation keeping costs. To constrain the rate, consider an augmented formulation of the original control law. In the initial development, the control input is introduced into the radial dynamics through

$$\ddot{r} = \frac{\dot{\bar{r}} \cdot \dot{\bar{r}}}{r} + \frac{\bar{r} \cdot \ddot{\bar{r}}}{r} - \frac{\bar{r} \cdot \dot{\bar{r}}}{r^2} \dot{r} \,. \tag{1.8}$$

It is straightforward to demonstrate that Equation (1.8) can also be written in the more familiar form,

$$\ddot{r} - r\dot{\theta}^2 = f_r + u_r \,. \tag{1.9}$$

The desired radial error dynamics are defined to follow a critically damped response, of natural frequency ω_n, such that the nominal radial response, $g_r\left(r,\dot{r}\right)$, is determined as,

$$\ddot{r} = g_r\left(r,\dot{r}\right) = \ddot{r}^* - 2\omega_n\left(\dot{r} - \dot{r}^*\right) - \omega_n^2\left(r - r^*\right). \tag{1.10}$$

Here, the superscript "$*$" implies evaluation on the nominal path (i.e. the desired vehicle separation).

The equation of motion relating the rotation rate to the control input is determined by differentiating the angular momentum vector expression. This operation leads to one equation of constraint, $u_h + f_h = 0$, as well as one additional equation of motion,

$$r\ddot{\theta} + 2\dot{r}\dot{\theta} = f_\theta + u_\theta \,. \tag{1.11}$$

In this particular example, the error dynamics for the rotation rate are specified as a decaying exponential, $\delta\dot{\theta} = \delta\dot{\theta}(0)e^{-k\omega_n t}$. The desired response, $g_\theta\left(\dot{\theta}\right)$, is then determined as

$$\ddot{\theta} = g_\theta\left(\dot{\theta}\right) = \ddot{\theta}^* - k\omega_n\left(\dot{\theta} - \dot{\theta}^*\right), \tag{1.12}$$

where k is an arbitrary scale factor and ω_n is the same natural frequency as in Equation (1.10). Substitution of Equation (1.12) into (1.11) and of (1.10) into (1.9) leads to the following scalar control laws

$$u_r\left(t\right) = g_r\left(r,\dot{r}\right) - f_r - r\dot{\theta}^2 \,, \tag{1.13}$$

$$u_\theta\left(t\right) = rg_\theta\left(\dot{\theta}\right) - f_\theta + 2\dot{r}\dot{\theta} \,, \tag{1.14}$$

$$u_h\left(t\right) = -f_h \;\left(\text{constraint}\right). \tag{1.15}$$

The control input that is actually applied to the deputy equations of motion, as listed in Equation (1.4), is then determined by transforming the input vector described by Equations (1.13)-(1.15) back into the ephemeris inertial frame,

$$\overline{u}_{D_i} = {}^{I}C^{E}\left[u_r \quad u_\theta \quad u_h\right]^T, \tag{1.16}$$

where ${}^{I}C^{E} = \left[\hat{r} \quad \hat{\theta} \quad \hat{h}\right]$. A sample implementation of this control law is illustrated in Figure 2 for a 700 kg spacecraft targeting a 5 km radial separation and rotation rates of one revolution every six or twenty-four hours. The initial state is the same as that in Figure 1(a).

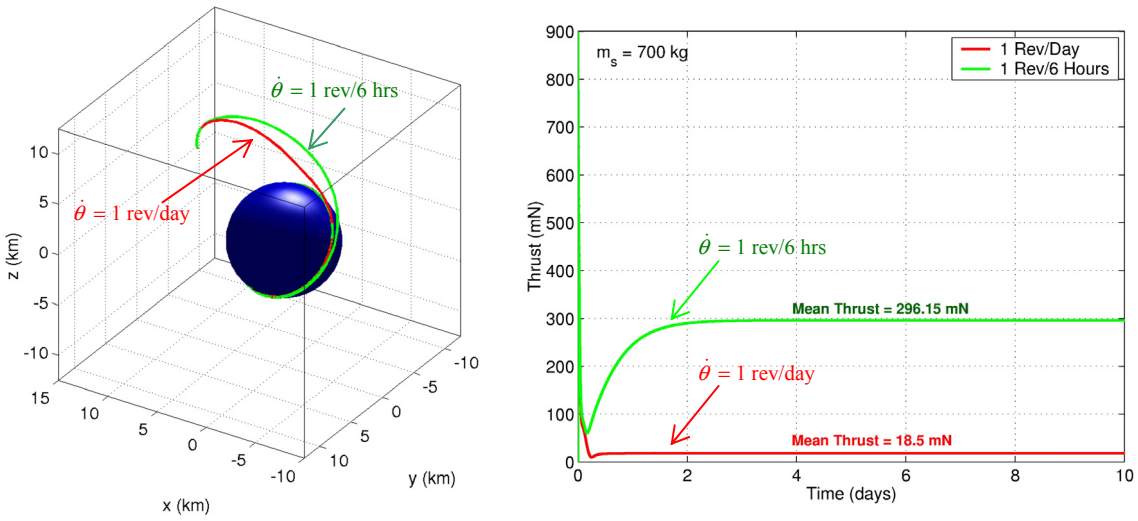

Figure 2 - OFL Control of Radial Distance + Rotation Rate and Associated Thrust Profile

Using this type of control law, it is possible to determine how the formation keeping cost varies both as a function of the commanded relative separation and the commanded rotation rate. As before, the equation of constraint guarantees that the plane of motion is entirely determined by the relative state of the deputy before the controller is activated. The associated trends in the cost are illustrated in Figure 3 in terms of the mean thrust required to enforce the formation. Note that the cost increases quadratically with increasing rotation rate and linearly with the separation that is commanded between the chief and deputy vehicles.

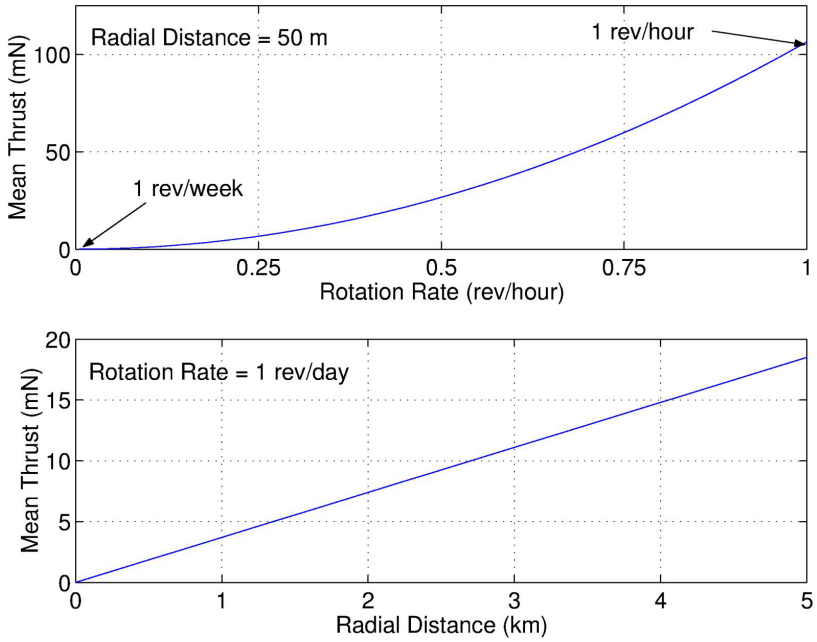

Figure 3 – Impact of Commanded Radial Distance and Spin Rate on Formation Keeping Costs

For a nominal separation of 50 meters, commanding the deputy to spin at one revolution per hour, about the chief spacecraft, requires over 100 mN of thrust, for a 700 kg vehicle. The mean thrust drops to 6.7 mN if the deputy vehicle is to nominally orbit the chief spacecraft once every 4 hours. The thrust levels continue to drop down to 0.19 mN for one revolution a day. If one revolution per day is required, a 500 meter separation raises the mean thrust to 18 mN.

Though the plane of motion is not affected by this type of control approach, activating the controller at the appropriate time, or biasing the initial velocity, may be sufficient to achieve the desired orbital plane. Overall, the control strategy is conceptually simple and numerically efficient for implementation in the ephemeris model. A more ambitious goal involving OFL control, then, is to target aspherical formations.

ASPHERICAL FORMATIONS

Consider a multi-spacecraft formation where the chief vehicle evolves along a quasi-periodic Lissajous trajectory near L_1 or L_2, as determined in the ephemeris model. The deputy vehicles in the formation are to follow the chief such that their relative motion evolves along the surface of a paraboloid that is inertially fixed in orientation. The chief spacecraft and the nadir of the paraboloid define the focal line of the formation. Maintenance of a constant distance between the chief vehicle and the nadir of the paraboloid is the first objective of the controller. The second requirement is that the motion of all deputies, even during reconfigurations, is constrained to evolve along the surface of the paraboloid. To accomplish these goals, it is first necessary to define a suitable parameterization for the formation surface. To that end, consider the illustration in Figure 4.

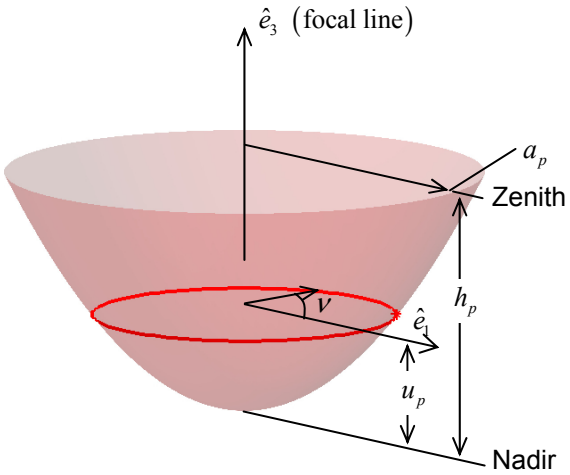

Figure 4 - Parameterization of a Paraboloid

The paraboloid in Figure 4 is defined in an inertial frame (*E*) described in terms of the unit vectors $\hat{e}_1$, $\hat{e}_2$, and $\hat{e}_3$. The orientation of this frame, relative to the ephemeris inertial frame (*I*), is defined by the azimuth (α) and elevation (δ) of the focal line relative to the inertial frame (*I*) unit vectors $\hat{X}$, $\hat{Y}$, and $\hat{Z}$. This is better visualized from Figure 5, where the unit vector $\hat{e}_3$ is directed from the chief vehicle to the nadir of the nominal paraboloid.

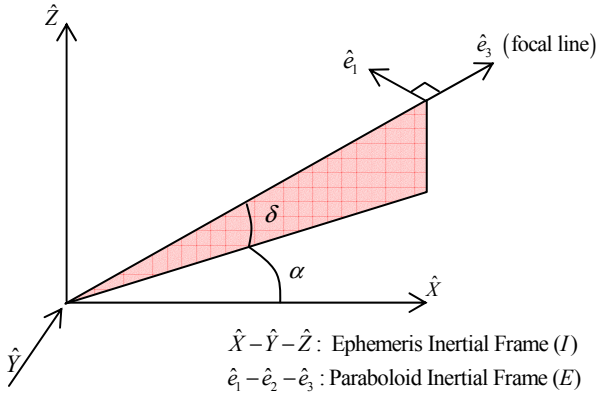

Figure 5 - Formation Focal Line Orientation

This direction is representative of the focal line of the formation. The "height" of any given deputy vehicle along this surface, measured relative to the nadir point, is defined by u_p where $0 \le u_p \le h_p$ and h_p denotes the maximum allowable height along the paraboloid. The radius at the zenith of the paraboloid ($u_p = h_p$) is denoted by the variable a_p. The unit vector $\hat{e}_1$, defined as $\hat{e}_1 = \hat{Z} \times \hat{e}_3 \big/ \left| \hat{Z} \times \hat{e}_3 \right|$, is simply a reference direction for the measurement of the angular position (ν) along the surface in Figure 1. Of course, $\hat{e}_2 = \hat{e}_3 \times \hat{e}_1$ completes the right handed inertial triad. The variables ν and u_p completely specify the position of a deputy vehicle along the formation surface in Figure 4. In the focal frame (*E*), the position vector from the nadir to any given deputy vehicle along the surface of the paraboloid is defined as

$$\overline{p}\left(u_p, \nu\right) = \left(a_p \sqrt{u_p / h_p}\, \cos\nu\right)\hat{e}_1 + \left(a_p \sqrt{u_p / h_p}\, \sin\nu\right)\hat{e}_2 + u_p \hat{e}_3 . \tag{1.17}$$

The desired position of the nadir, relative to the chief spacecraft, is specified as $\overline{q} = q\hat{e}_3$. The equation of motion in (1.5) is associated with the inertial frame (*I*). The nominal relative position vector can also be written in terms of *E*-frame coordinates as $\overline{\rho}_E = \overline{q} + \overline{p}\left(u_p, \nu\right)$. In this alternate inertial frame, the nominal relative acceleration vector, ${}^E\ddot{\overline{\rho}}_E$, can be expressed as

$${}^E\ddot{\overline{\rho}}_E = {}^E\ddot{\overline{q}} + \left(\overline{p}_{u_p u_p}\dot{u}_p + \overline{p}_{u_p \nu}\dot{\nu}\right)\dot{u}_p + \overline{p}_{u_p}\ddot{u}_p + \left(\overline{p}_{\nu u_p}\dot{u}_p + \overline{p}_{\nu\nu}\dot{\nu}\right)\dot{\nu} + \overline{p}_{\nu}\ddot{\nu} , \tag{1.18}$$

where $\bar{p}_{u_p}$, $\bar{p}_{u_p u_p}$, $\bar{p}_{u_p \nu}$, $\bar{p}_{\nu u_p}$, $\bar{p}_{\nu}$, and $\bar{p}_{\nu\nu}$ denote the first and second partial derivatives of $\bar{p}$ with respect to u_p and ν, respectively. The scalar rates $\dot{u}_p$ and $\dot{\nu}$ represent the climb rate and the rotation rate along the nominal surface. Since both the *E* and *I* frames are inertial, the accelerations in Equations (1.5) and (1.18) are related through the orientation matrix ${}^{I}C^{E}$ such that ${}^{I}\ddot{\bar{\rho}}_{I} = \left\{ {}^{I}C^{E} \right\} {}^{E}\ddot{\bar{\rho}}_{E}$. The j^{th} column of the matrix ${}^{I}C^{E}$ corresponds to the unit vector $\hat{e}_j$, for $j = 1-3$, defined in Figure 5.

In order for the nominal motion to satisfy Equation (1.18) precisely, the control law must be applied continuously and is determined as

$$\bar{u}^{\circ}_{D_i}(t) = \left\{ {}^{i}C^{e} \right\} \left[{}^{e}\ddot{\bar{q}} + \left(\bar{p}_{u_p} \ddot{u}_p + \bar{p}_{\nu} \ddot{\nu} \right) + \left(\bar{p}_{u_p u_p} \dot{u}_p{}^2 + 2\bar{p}_{u_p \nu} \dot{u}_p \dot{\nu} + \bar{p}_{\nu\nu} \dot{\nu}^2 \right) \right] - \Delta\bar{f}\left(\bar{r}_I \right). \tag{1.19}$$

Consider a formation characterized by $\bar{q} = (10\text{ km})\hat{e}_3$, $h_p = 500$ m, $a_p = 500$ m. Let the focal line be oriented such that $\alpha = 0^{\circ}$, and $\delta = 45^{\circ}$. Each vehicle in the formation is to complete one revolution along the surface once a day, $\dot{\nu} = 1$ rev/day. The nominal motion of one of the vehicles is initially described by $u_p = 200$ meters such that $\dot{u}_p = \ddot{u}_p = 0$ and $\ddot{\nu} = 0$. After 5 days, the vehicle's nominal path must be reconfigured, along the paraboloid, such that $\dot{\nu}$ and $\dot{u}_p$ remain constant. The climb rate, $\dot{u}_p$, is specified such that, after 1 day, the vehicle has raised it's "height" to 500 meters relative to the nadir of the paraboloid, a 300 meter climb relative to the initial orbit. The nominal control law in Equation (1.19) leads to the desired motion as illustrated in Figure 6.

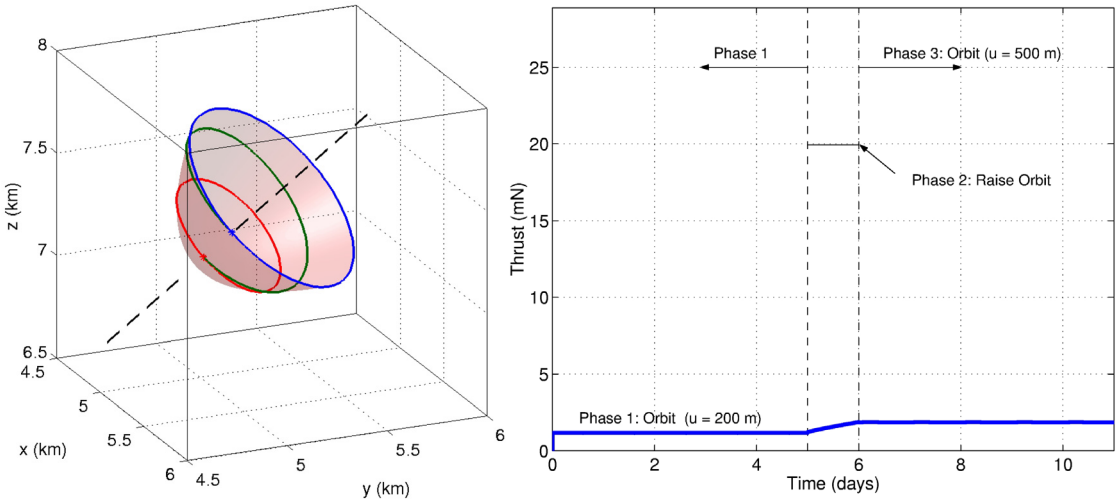

Figure 6 – Nominal Geometry and Thrust Requirements for a Sample Parabolic Formation

In this Figure, the off-center circular orbit closest to the nadir (red) represents the initial nominal motion over a span of 5 days. The green spiral defines the reconfiguration segment over the next day while the highest circular orbit (blue) denotes the converged solution over the remaining 5 days. The associated nominal thrust profile reveals that a range of 1.4 to 2.0 mN of thrust is required to enforce the formation, including the reconfiguration, in the absence of external perturbations.

Output Feedback Linearization: Application to Parabolic Formations

The control design presented above is associated with nominal formation keeping. That is, assuming the vehicles are already in the desired configuration, Equation (1.19) establishes the thrust profile necessary to enforce the desired formation continuously. In the example illustrated in Figure 6, each phase is computed separately and independently from the other. For instance, the end-state of Phase I, plus the necessary impulsive ΔV, is used as the initial state to compute the trajectory associated with Phase II. A similar approach is employed to determine the trajectory associated with Phase III. Hence, the above solution addresses neither the deployment nor the reconfiguration of an actual continuous solution. To address this aspect, output feedback linearization techniques are applied.

In prior investigations, input/output feedback linearization (IFL/OFL) is successfully applied to achieve the desired formation keeping goals. The earlier OFL examples are based on a tracking scheme involving relative distance and rotation rate. Hence, the number of variables to track is less than the number of available control inputs. As such, there are an infinite number of solutions available that satisfy the goals of the controller. In the present case, a parabolic configuration requires the tracking of three variables: $u_p(t)$, $q(t)$, and $\nu(t)$. That is, the distance to the nadir, the height of the vehicle along the paraboloid surface and the orientation time history along the surface. To illustrate how an OFL controller may be applied to this type of configuration, it is necessary to establish a set of expressions relating the state variables (and control inputs) to the tracked quantities. For instance, recall that

$$\bar{\rho}_I = {}^I C^E \bar{\rho}_E = \begin{bmatrix} \tilde{x} & \tilde{y} & \tilde{z} \end{bmatrix}^T, \tag{1.20}$$

where the symbol '~' above each variable indicates that the measure numbers are associated with the focal frame (E) of the paraboloid.

These measure numbers are related to the paraboloid parameters in Figure 4 as follows,

$$\tilde{x} = a_p \sqrt{u_p / h_p} \cos\nu \,, \tag{1.21}$$

$$\tilde{y} = a_p \sqrt{u_p / h_p} \sin\nu \,, \tag{1.22}$$

$$\tilde{z} = q + u_p \,. \tag{1.23}$$

Squaring and then adding Equations (1.21)-(1.22) reveals that

$$u_p = \left(h_p / {a_p}^2\right)\left[\tilde{x}^2 + \tilde{y}^2\right], \tag{1.24}$$

while dividing Equation (1.22) by Equation (1.21) yields

$$\tan\nu = \left(\tilde{y} / \tilde{x}\right). \tag{1.25}$$

Furthermore, Equation (1.23) indicates that

$$q = \tilde{z} - \left(h_p / {a_p}^2\right)\left[\tilde{x}^2 + \tilde{y}^2\right]. \tag{1.26}$$

The associated rates are defined by differentiating Equations (1.24)-(1.26) with respect to time, i.e.,

$$\dot{u}_p = \frac{2h_p}{{a_p}^2}\left(\tilde{x}\dot{\tilde{x}} + \tilde{y}\dot{\tilde{y}}\right), \tag{1.27}$$

$$\dot{q} = \dot{\tilde{z}} - \frac{2h_p}{{a_p}^2}\left(\tilde{x}\dot{\tilde{x}} + \tilde{y}\dot{\tilde{y}}\right), \tag{1.28}$$

$$\dot{\nu} = \frac{\tilde{x}\dot{\tilde{y}} - \tilde{y}\dot{\tilde{x}}}{\left(\tilde{x}^2 + \tilde{y}^2\right)}. \tag{1.29}$$

With these expressions, it is possible to identify relationships between the control inputs and the tracked variables. These relationships are obtained by differentiating Equations (1.24)-(1.26) twice with respect to time. Differentiation is straightforward and ultimately suggests that,

$$g_{u_p}\left(u_p, \dot{u}_p\right) - \frac{2h_p}{{a_p}^2}\left(\dot{\tilde{x}}^2 + \dot{\tilde{y}}^2 + \tilde{x}\Delta\tilde{f}_x + \tilde{y}\Delta\tilde{f}_y\right) = \frac{2h_p}{{a_p}^2}\tilde{x}\tilde{u}_x + \frac{2h_p}{{a_p}^2}\tilde{y}\tilde{u}_y \,. \tag{1.30}$$

$$g_q\left(q, \dot{q}\right) + \frac{2h_p}{{a_p}^2}\left(\dot{\tilde{x}}^2 + \dot{\tilde{y}}^2 + \tilde{x}\Delta\tilde{f}_x + \tilde{y}\Delta\tilde{f}_y\right) - \Delta\tilde{f}_z = -\frac{2h_p}{{a_p}^2}\tilde{x}\tilde{u}_x - \frac{2h_p}{{a_p}^2}\tilde{y}\tilde{u}_y + \tilde{u}_z \tag{1.31}$$

$$g_{\dot{\nu}}\left(\dot{\nu}\right) + 2\frac{\left(\tilde{x}\dot{\tilde{x}} + \tilde{y}\dot{\tilde{y}}\right)\left(\tilde{x}\dot{\tilde{y}} - \tilde{y}\dot{\tilde{x}}\right)}{\left(\tilde{x}^2 + \tilde{y}^2\right)^2} + \frac{\left(\tilde{y}\Delta\tilde{f}_x - \tilde{x}\Delta\tilde{f}_y\right)}{\left(\tilde{x}^2 + \tilde{y}^2\right)} = \frac{\tilde{x}}{\left(\tilde{x}^2 + \tilde{y}^2\right)}\tilde{u}_y - \frac{\tilde{y}}{\left(\tilde{x}^2 + \tilde{y}^2\right)}\tilde{u}_x \tag{1.32}$$

In Equations (1.30)-(1.32), recall that the '~' represents quantities associated with the focal frame (*E*) of the paraboloid. Hence, $\tilde{u} = {}^{E}C^{I}\bar{u} = \begin{bmatrix} \tilde{u}_x & \tilde{u}_y & \tilde{u}_z \end{bmatrix}^T$ represents the transformed control input vector. Similarly, $\Delta\tilde{f} = {}^{E}C^{I}\Delta\bar{f}^{(D_i)} = \begin{bmatrix} \Delta\tilde{f}_x & \Delta\tilde{f}_y & \Delta\tilde{f}_z \end{bmatrix}^T$ and $\tilde{r} = {}^{E}C^{I}\bar{r} = \begin{bmatrix} \tilde{x} & \tilde{y} & \tilde{z} \end{bmatrix}^T$ denote the differential force and the radial distance to the chief spacecraft, in terms of focal frame coordinates, respectively. The scalar functions $g_{u_p}\left(u_p, \dot{u}_p\right)$, $g_q\left(q, \dot{q}\right)$ and $g_{\dot{\nu}}\left(\dot{\nu}\right)$ reflect the desired dynamical response for the variables u_p, q, and $\dot{\nu}$. As an example, critically damped error dynamics are desired for the distance elements u_p and q while an exponentially decaying error response is sought for $\dot{\nu}$.

An exact solution is available for Equations (1.30)-(1.32). To simplify the form of the solution, let $\alpha_x = 2h_p\tilde{x}/{a_p}^2$, $\alpha_y = 2h_p\tilde{y}/{a_p}^2$, $\beta_x = \tilde{x}/\left(\tilde{x}^2 + \tilde{y}^2\right)$, and $\beta_y = \tilde{y}/\left(\tilde{x}^2 + \tilde{y}^2\right)$. Furthermore, let the left hand side of Equations (1.30)-(1.32) be summarized by G_{u_p}, G_q, and $G_{\dot{\nu}}$, respectively. Then, the commanded control input is expressed

$$\tilde{u}_x = \frac{\left(\beta_x G_{u_p} - \alpha_y G_{\dot{\nu}}\right)}{\left(\alpha_x\beta_x + \alpha_y\beta_y\right)}, \tag{1.33}$$

$$\tilde{u}_y = \frac{\left(\beta_y G_{u_p} + \alpha_x G_{\dot{\nu}}\right)}{\left(\beta_x\alpha_x + \beta_y\alpha_y\right)}, \tag{1.34}$$

$$\tilde{u}_z = G_{u_p} + G_q. \tag{1.35}$$

Note, the above control law is singular if the deputy crosses the focal line ($\hat{e}_3$), $\tilde{x} = \tilde{y} = 0$. This does not present a significant issue, however, because once the deputy is on the surface of the paraboloid this condition is never met. This singularity can only occur while the deputy is being driven onto the surface during the injection phase. To circumvent this difficulty, it is only necessary to allow the vehicle to coast away from this point before reactivating the controller.

For implementation of this approach in the ephemeris model, the integration of each vehicle proceeds separately in an Earth centered inertial frame (*I*). The relative state of the deputy with respect to the chief is computed from these Earth centered states. These quantities are then transformed into the focal frame (*E*) via $\tilde{r} = {}^{E}C^{I}\bar{r}$ and $\dot{\tilde{r}} = {}^{E}C^{I}\dot{\bar{r}}$. The results of this transformation are substituted into Equations (1.24)-(1.29) to determine the values of the quantities to be tracked as well as the necessary control accelerations, as computed from Equations (1.33)-(1.35).

To illustrate the application of this approach, consider the nominal sample scenario previously introduced and depicted in Figure 6. An injection error is introduced such that the initial relative state of the deputy, with respect to the chief spacecraft, is characterized by $\bar{r} = \left(4.6\hat{X} + 4.3\hat{Y} + 6.934\hat{Z}\right)$ km with a relative velocity defined by $\dot{\bar{r}} = 0.05\hat{X} - 0.05\hat{Y} - 0.05\hat{Z}$ m/sec. This particular initial state is arbitrarily selected to facilitate the visualization process. For any arbitrary initial state, the controller should drive the vehicles in the formation to the initial configuration, then reconfigure at the appropriate time. Once deployed, this evolution is to proceed along the surface of the paraboloid. Application of this controller results in the trajectory illustrated in Figure 7.

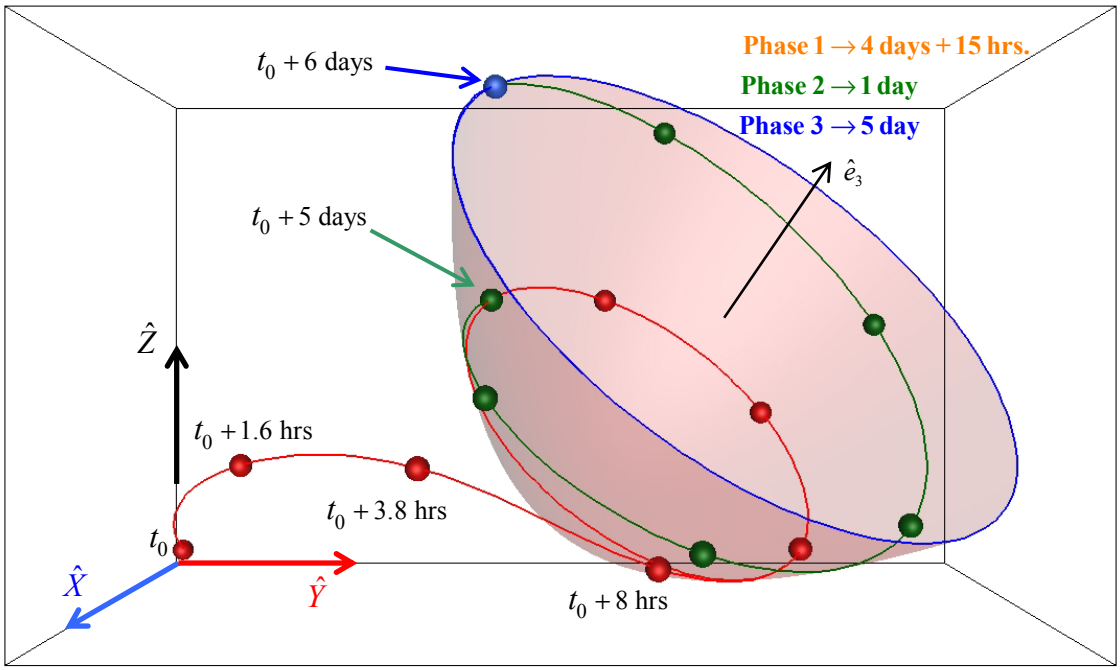

Figure 7 – OFL Controlled Parabolic Formation

The resulting path is divided into three segments. The segment highlighted in orange represents the injection phase as well as the initial orbit phase, for $u_p = 200$ m. The green segment denotes the reconfiguration phase, characterized by $\dot{u}_p = 300$ meters/day. The last segment, in blue, is the final phase associated with $u_p = 500$ m. The thrust profile associated with this solution appears in Figure 8. Note that, at the present stage of development, each vehicle is controlled separately. Future studies must incorporate relative information between deputies to assess the probability of collisions.

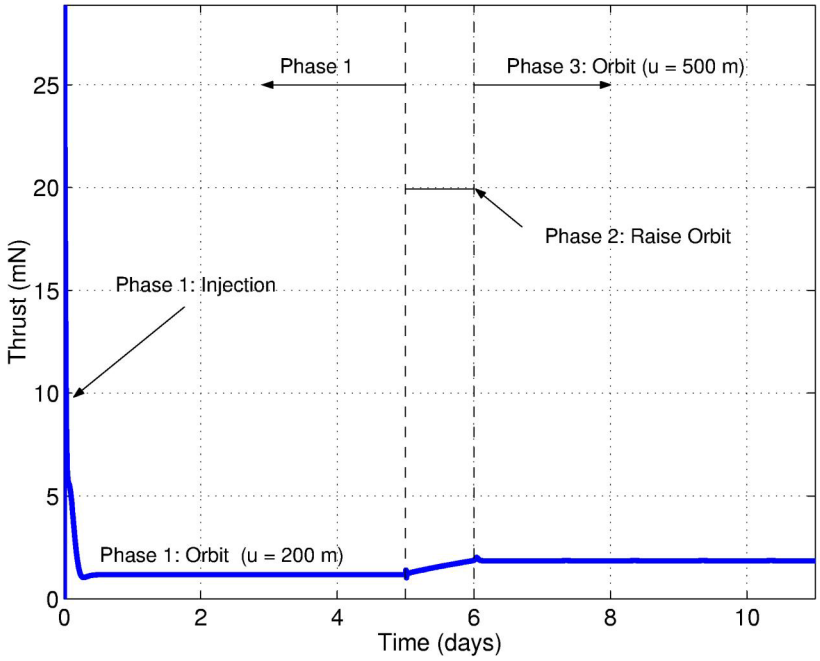

Figure 8 - Thrust Profile for OFL Controlled Parabolic Formation

Comparing Figure 6 to Figure 8, it is clear that the OFL controller converges to the nominal control except for the initial correction that is necessary for injection into the nominal configuration. The thrust levels range from 25mN during injection to 1-2 mN for orbit maintenance. Note that the maximum thrust amplitude will vary according to the response frequency that is specified. Also, though both the nominal and actual thrust profiles, appear to converge onto constant segments, there is an oscillation on the order of 0.003 mN during the orbit phase at $u_p = 200$ (last part of Phase 1) m and $u_p = 500$ m (Phase 3). Unlike the configurations previously considered, the chief spacecraft, in this case, is not the center of the formation.

NATURAL AND NON-NATURAL FORMATIONS IN THE EPHEMERIS MODEL

Besides the non-natural formations identified in the previous discussion, there exist some natural relative behaviors that can be exposed and potentially exploited for formations. For example, a variety of natural formations can be isolated through knowledge of the dynamical flow near a "halo" orbit. Howell and Barden [6-7] identify a planar formation in which individual vehicles evolve along the surface of a two-dimensional hollow torus. The vehicles always remain in a plane although the formation expands and contracts and the plane changes orientation.

This torus is known to envelop the reference "halo" orbit in the CR3BP. This type of solution also exists in the ephemeris model and can be identified, numerically, via a two-level differential correction process, such as that developed by Howell and Pernicka [20].

The relative dynamics associated with the torus are determined from a center manifold analysis, based on the linear stability properties of the reference solution, that is, the reference halo orbit. The reference halo orbits that are of interest for spacecraft missions are usually unstable. The stability of such an orbit is characterized by one stable and one unstable mode, as well as four center modes. The torus formation identified by Howell and Barden [6-7], appearing in Figure 9(a), is associated with two of these center modes.

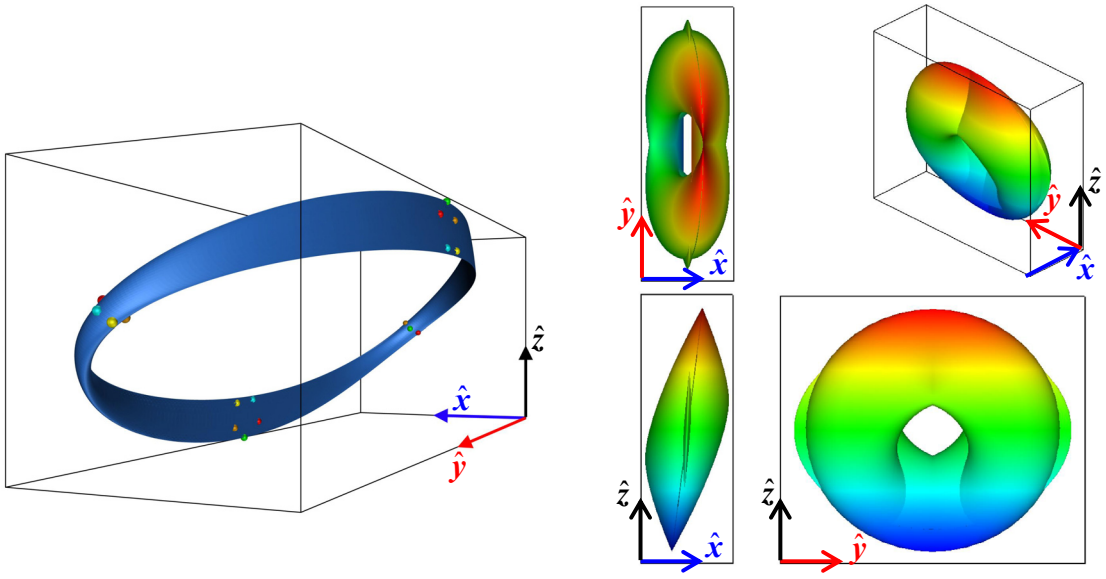

(a) (b)

Figure 9 - Natural Quasi-periodic Formation Associated with Reference Halo Orbit

The reference halo orbit evolves along the interior (center) of this two-dimensional hollow torus. Relative to the chief spacecraft, evolving along this reference halo orbit, the deputy motion is constrained to evolve along the surface depicted in Figure 9(b). The surfaces in Figure 9(a-b) are representative of the same motion as seen by different observers. Figure 9(a), for instance, is indicative of the motion of the deputy vehicle (*D*) as seen by an observer fixed at the libration point (L_i), $\bar{r}^{L_iD}$. Figure 9(b), then, is representative of the motion of the deputy vehicle (D), as observed by the chief spacecraft (*C*) as it evolves along the reference halo orbit, $\bar{r}^{L_iD} - \bar{r}^{L_iC}$.

The remaining two center modes lead to nearby periodic halo orbits. The relative motion associated with these two center modes reveals the existence of periodic and slowly expanding relative orbits, depending on the target state within the new subspace, as demonstrated by Marchand and Howell [14]. The approximate period of these relative solutions is close to that of the reference halo (~180 days). Figure 10 illustrates the projection onto the rotating *yz*-plane of a sample set of these solutions, as determined in the CR3BP. Note, the blue sphere in Figure 10 represents the chief spacecraft but is greatly enlarged for ease of visualization.

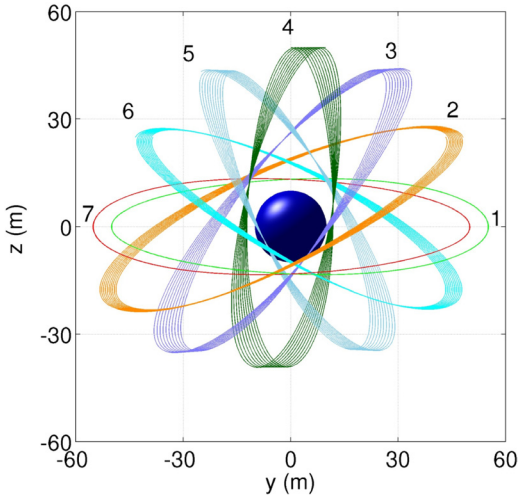

Figure 10 - Periodic and Slowly Expanding Relative Orbits in the CR3BP

In Figure 9(b) and Figure 10, the chief spacecraft is located at the origin. The methodology implemented by Marchand and Howell [14], based on Floquet theory, is used to numerically identify these relative orbits in the CR3BP. The same procedure is used as an impulsive control scheme to deploy spacecraft into these natural solutions through a single injection maneuver. In the current work, these solutions are transitioned into the ephemeris model using a two-level corrector [20]. For the nearly periodic solutions, the resulting motion is essentially unchanged by the transition, as seen from Figure 11(a). Even the addition of solar radiation pressure does not appear to have a significant impact, depending on the spacecraft mass and effective area, of course. However, as the orientation of the relative orbit is shifted towards the vertical orbits, Figure 11(b-c), the impact of SRP is much more visible.

These naturally existing motions can be used as initial guesses to compute non-natural formations. In this initial investigation, assume that only impulsive control is available to achieve the objective. For instance, consider the orbit in Figure 11(c). The relative path is clearly not periodic but, the initial guess is sufficiently close to periodic if the effects of SRP are small.

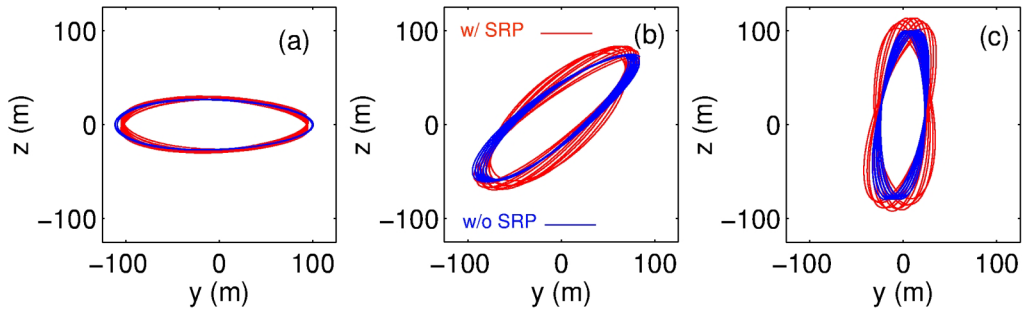

Figure 11 – Natural Formations in the Ephemeris Model
Impact of Solar Radiation Pressure (SRP)

In this case, a differential corrector can be applied to enforce periodicity if impulsive maneuvers are allowed. The process is similar to a method commonly used to transition halo orbits into the ephemeris model. Consider the first two revolutions of the path (without SRP) in Figure 11(b). A two-level differential corrections process, in this case with initial- and end-point constraints, determines the maneuver necessary to close the orbit over this time period. The patch points associated with the converged solution are then shifted forward in time to add *N* additional revolutions. The complete solution is then differentially corrected while allowing maneuvers at the intersections between revolutions. A sample solution, over six revolutions, is illustrated in Figure 0 and is obtained by applying two impulsive maneuvers ranging in size from 2.5 m/sec to 5 m/sec at the specified locations.

A similar approach can be applied to the nearly vertical trajectory in Figure 11(c) to obtain vertical periodic relative orbits, as illustrated in Figure 13. This particular approach works very well if periodicity is enforced in the rotating frame, as opposed to the inertial frame. Relative to an observer fixed in the rotating frame, these solutions appear to be sufficiently close to periodic and are, subsequently, a suitable initial guess for the differential corrector. However, the associated inertial perspectives, illustrated in Figure 14, are quite different. Thus far, these do not appear to provide a sufficiently accurate initial guess if periodicity is required. That is because of the natural geometry of the solution and the fact that the Earth is at a different location every time a revolution is completed, as opposed to a perspective originating in the rotating frame. At the present time, however, no conclusive statements can be made since this is still a subject of ongoing study.

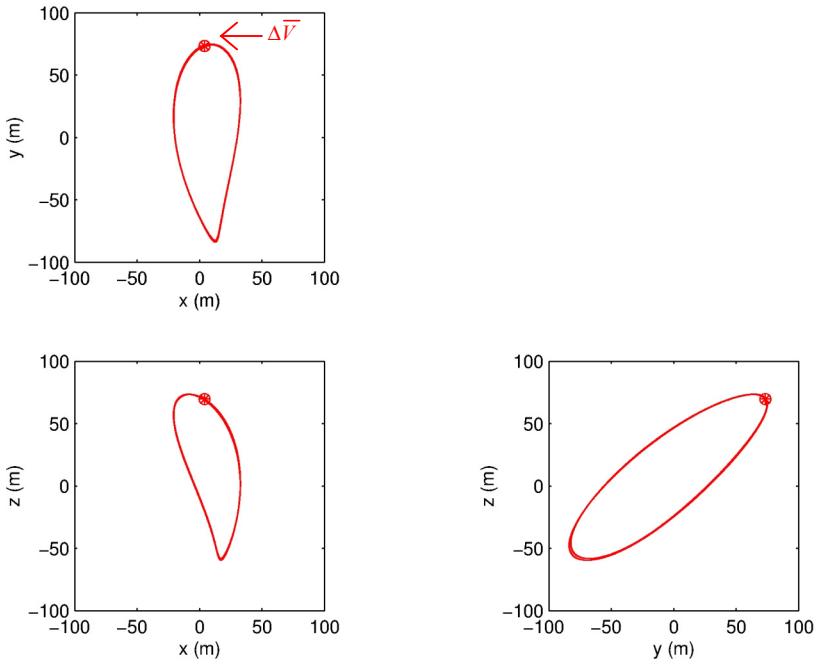

Figure 12 – Controlled Periodic Orbit in the Ephemeris Model (w/o SRP)

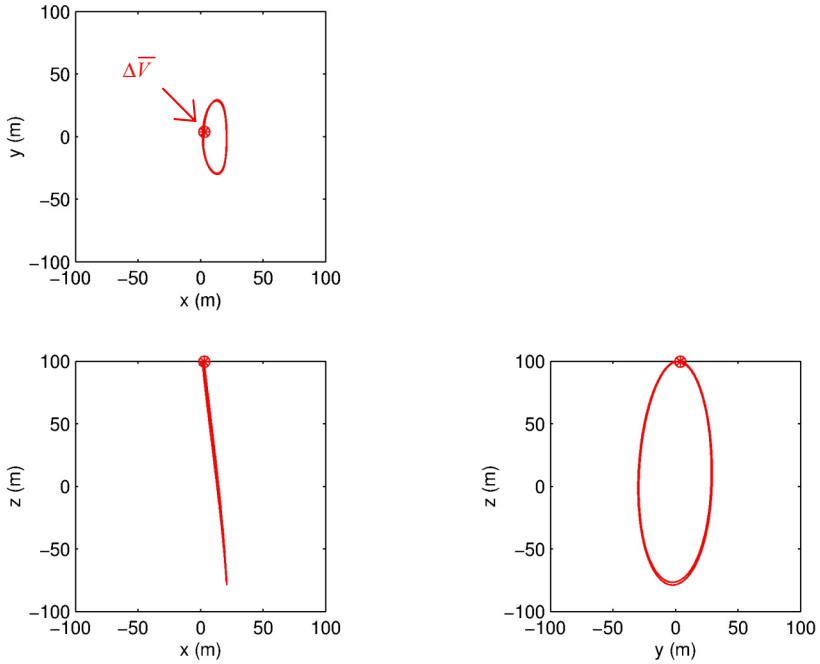

Figure 13 – Controlled Vertical Orbits in the Ephemeris Model (w/o SRP)

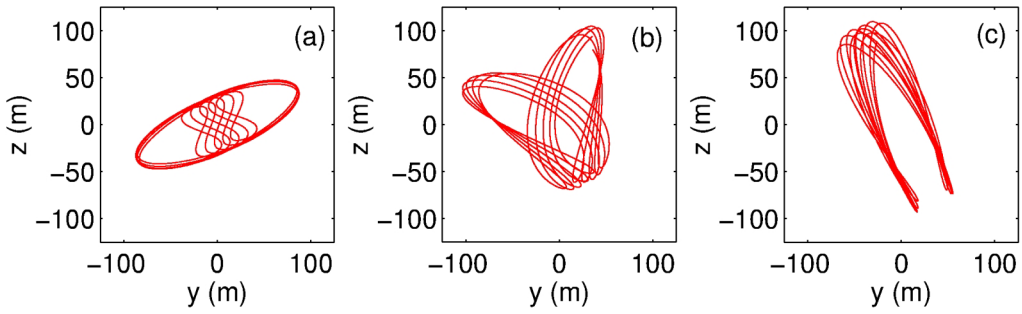

Figure 14 – Natural Formations in the Ephemeris Model
Inertial Frame Perspective of Figures 11(a-c) (w/ SRP)

CONCLUSIONS

In the present investigation, output feedback linearization (OFL) techniques are successfully applied to deploy, enforce, and reconfigure spherical and aspherical formations near the vicinity of the libration points of the Sun-Earth/Moon system. All the control laws considered are developed and implemented in the full ephemeris model including solar radiation pressure and any number of desired gravitational perturbations. Depending on the constraints imposed on the formation, the results presented in this study often require thrust levels on the order of milli-Newton's for a 700 kg spacecraft. In contrast, the deployment phase can require thrust levels in the Newton range, depending on when the controller is activated. This range of thrust levels appears to be achievable with presently available technology. However, currently, these technologies are mostly devoted to station keeping and attitude control, which does not often require long term operation. Hence, the lifetime of the propulsion system, within the context of the configurations defined here, may require further enhancements. Even if the formation constraints can be met, theoretically, the sensitivity of these methods to modeling and thruster implementation errors must be addressed. This is of particular importance for libration point missions given the associated dynamical sensitivities to small perturbations. Certainly, on any of the examples presented here, discontinuing the thrust input at any time, or placing bounds on its amplitude, leads to divergence from the desired nominal, especially with the higher rates of rotation that induce higher tangential speeds.

Another area of interest in this study is the use of naturally existing configurations to construct non-natural formations via impulsive control. The methods associated with the determination of these natural solutions are determined from center manifold analysis and the application of a previously developed Floquet controller to deploy into these configurations. Thus far, the method presented is only applied to establish periodic vertical relative orbits in the ephemeris model. These and other techniques are still under study regarding configurations that are, in some general sense, fixed relative to the inertial frame.

The knowledge gained from the application of the continuous (OFL Controller) and impulsive techniques (Floquet Controller) can potentially, be applied as a combined formation keeping strategy. That is, if the formation goals only require the nominal configuration to be maintained over a predetermined time interval, the Floquet controller can be used to place the vehicles into natural formations until the next reconfiguration is necessary. At this point, the continuous controller can once again be activated to return the vehicles into the desired configuration.

ACKNOWLEDGEMENTS

This research was carried out at Purdue University with support from the Clare Boothe Luce Foundation and the National Aeronautics and Space Administration, Contract Number NCC5-727.

REFERENCES

[1] D.J. Scheeres and N.X. Vinh, "Dynamics and control of relative motion in an unstable orbit." AIAA/AAS Astrodynamics Specialist Conference, Denver, Colorado, Aug. 14-17, 2000. AIAA Paper No. 2000-4135.

[2] P. Gurfil and N. J. Kasdin, "Dynamics and Control of Spacecraft Formation Flying in Three-Body Trajectories." AIAA Guidance, Navigation, and Control Conference and Exhibit, Montreal, Canada, Aug. 6-9, 2001. AIAA Paper No. 2001-4026.

[3] P. Gurfil, M. Idan, and N. J. Kasdin, "Adaptive Neural Control of Deep-Space Formation Flying." American Control Conference (ACC), Proceedings. Vol. 4, Anchorage, Alaska, May 8-10, 2002, p. 2842-2847.

[4] N.H. Hamilton, "Formation Flying Satellite Control Around the L2 Sun-Earth Libration Point." M.S. Thesis, George Washington University, Washington, DC, December 2001.

[5] D. Folta, J.R. Carpenter, and C. Wagner, "Formation Flying with Decentralized Control in Libration Point Orbits." International Symposium: Spaceflight Dynamics, Biarritz, France, June, 2000.

[6] B.T. Barden and K.C. Howell, "Fundamental Motions Near Collinear Libration Points and Their Transitions." The Journal of the Astronautical Sciences, Vol. 46, No. 4, 1998, pp. 361-378.

[7] B.T. Barden, and K.C. Howell, "Formation Flying in the Vicinity of Libration Point Orbits." Advances in Astronautical Sciences, Vol. 99, Pt. 2, 1998, pp. 969-988.

[8] B.T. Barden and K.C. Howell, "Dynamical Issues Associated with Relative Configurations of Multiple Spacecraft Near the Sun-Earth/Moon L_1 Point." AAS/AIAA Astrodynamics Specialists Conference, Girdwood, Alaska, August 16-19, 1999, AAS Paper No. AAS99-450.

[9] K.C. Howell and B.T. Barden, "Trajectory Design and Stationkeeping for Multiple Spacecraft in Formation Near the Sun-Earth L_1 Point." IAF 50th International Astronautical Congress, Amsterdam, Netherlands, Oct. 4-8, 1999. IAF/IAA Paper No. 99-A707.

[10] G. Gómez, M. Lo, J. Masdemont, and K. Museth, "Simulation of Formation Flight Near Lagrange Points for the TPF Mission." AAS/AIAA Astrodynamics Conference, Quebec, Canada, July 30-Aug. 2, 2001. AAS Paper No. 01-305.

[11] K.C. Howell and T. Keeter, "Station-Keeping Strategies for Libration Point Orbits - Target Point and Floquet Mode Approaches." Advances in the Astronautical Sciences, Vol. 89, pt. 2, 1995, pp. 1377-1396.

[12] G. Gómez, K.C. Howell, J. Masdemont, and C. Simó, "Station-keeping Strategies for Translunar Libration Point Orbits." Advances in Astronautical Sciences, Vol. 99, Pt. 2, 1998, pp. 949-967

[13] K.C. Howell and B.G. Marchand, "Control Strategies for Formation Flight in the Vicinity of the Libration Points." AIAA/AAS Space Flight Mechanics Conference, Ponce, Puerto Rico, Feb. 9-13, 2003. AAS Paper No. 03-113.

[14] B.G. Marchand and K.C. Howell, "Formation Flight Near L_1 and L_2 in the Sun-Earth/Moon Ephemeris System Including Solar Radiation Pressure." AAS/AIAA Astrodynamics Specialists Conference, Big Sky, Montana, August 3-8, 2003. AAS Paper No. 03-596.

[15] K.C. Howell and B.G. Marchand, "Design and Control of Formations Near the Libration Points of the Sun-Earth/Moon Ephemeris System." 2003 Space Flight Mechanics Symposium – Goddard Space Flight Center, Greenbelt, MD.

[16] EO-1 Pulsed Plasma Thruster, http://space-power.grc.nasa.gov/ppo/projects/eo1/eo1-ppt.html.

[17] J. Mueller, "Thruster Options for Microspacecraft: A Review and Evaluation of Existing Hardware and Emerging Technologies." AIAA/ASME/SAE/ASEE Joint Propulsion Conference & Exhibit, 33rd, Seattle, WA, July 6-9, 1997. AIAA Paper No. 97-3058.

[18] A. D. Gonzales and R. P. Baker, "Microchip Laser Propulsion for Small Satellites." AIAA/ ASME/ SAE/ ASEE Joint Propulsion Conference and Exhibit, 37th, Salt Lake City, UT, July 8-11, 2001. AIAA Paper No. 2001-3789.

[19] C. Phipps and J. Luke, "Diode Laser-Driven Microthrusters - A New Departure for Micropropulsion." AIAA Journal, Vol. 40, No. 2, Feb. 2002, p. 310-318.

[20] K.C. Howell and H. J. Pernicka, "Numerical Determination of Lissajous Trajectories in the Restricted Three Body Problem." Celestial Mechanics, Vol. 41, pp. 107-124, 1988.